REPORT DOCUMENTATION PAGE

Form Approved
OMB No. 0704-0188

1. REPORT DATE *(DD-MM-YYYY)*
21-11-2005

REPRINT

4. TITLE AND SUBTITLE
AN EFFICIENT AND ACCURATE QUANTUM LATTICE-GAS MODEL FOR THE MANY-BODY SCHROEDINGER WAVE EQUATION

5a. CONTRACT NUMBER

5b. GRANT NUMBER

5c. PROGRAM ELEMENT NUMBER
61102F

6. AUTHOR(S)
J. Yepez and B. Boghosian*

5d. PROJECT NUMBER
2304

5e. TASK NUMBER
0T

5f. WORK UNIT NUMBER
B1

7. PERFORMING ORGANIZATION NAME(S) AND ADDRESS(ES)
Air Force Research Laboratory/VSBYA
29 Randolph Road
Hanscom AFB MA 01731-3010

8. PERFORMING ORGANIZATION REPORT NUMBER
AFRL-VS-HA-TR-2005-1169

9. SPONSORING / MONITORING AGENCY NAME(S) AND ADDRESS(ES)

10. SPONSOR/MONITOR'S ACRONYM(S)

11. SPONSOR/MONITOR'S REPORT NUMBER(S)

12. DISTRIBUTION / AVAILABILITY STATEMENT
Approved for Public Release; Distribution Unlimited.

*Dept of Mathematics, Tufts Univ, Medford, MA

13. SUPPLEMENTARY NOTES
REPRINTED FROM: COMPUTER PHYSICS COMMUNICATIONS, Vol 146, Issue 3 (2002), pp 339-344.

14. ABSTRACT

Presented is quantum lattice-gas model for simulating the time-dependent evolution of a many-body quantum mechanical system of particles governed by the non-relativistic Schroedinger wave equation with an external scalar potential. A variety of computational demonstrations are given where the numerical predictions are compared with exact analytical solutions. In all cases, the model results accurately agree with the analytical predictions and we show that the model's error is second-order in the temporal discretization and fourth-order in the spatial discretization. The difficult problem of simulating a system of fermionic particles is also treated and a general computational formulation of this problem is given. For pedagogical purposes, the two-particle case is presented and the numerical dispersion of the simulated wave packets is compared with the analytical solutions.

15. SUBJECT TERM:
Schroedinger wave equation Quantum computing Quantum lattice gas
Quantum mechanics Computational physics

16. SECURITY CLASSIFICATION OF:			17. LIMITATION OF ABSTRACT	18. NUMBER OF PAGES	19a. NAME OF RESPONSIBLE PERSON
a. REPORT		c. THIS PAGE			Jeffrey Yepez
UNCLAS	UNCLAS	UNCLAS	SAR		19b. TELEPHONE NUMBER *(include area code)* 781-377-5957

Computer Physics Communications Vol. 146, Issue 3 (2002) pages 339-344 Version 1.5

An efficient and accurate quantum lattice-gas model for the many-body Schroedinger wave equation

Jeffrey Yepez*
Air Force Research Laboratory, Hanscom AFB, Massachusetts
Jeffrey.Yepez@hanscom.af.mil
http://qubit.plh.af.mil/

Bruce Boghosian*
Department of Mathematics
Bromfield-Pearson Hall, Tufts University
Bruce.Boghosian@tufts.edu

23 April 2001

Abstract

Presented is quantum lattice-gas model for simulating the time-dependent evolution of a many-body quantum mechanical system of particles governed by the non-relativistic Schroedinger wave equation with an external scalar potential. A variety of computational demonstrations are given where the numerical predictions are compared with exact analytical solutions. In all cases, the model results accurately agree with the analytical predictions and we show that the model's error is second-order in the temporal discretization and fourth-order in the spatial discretization. The difficult problem of simulating a system of fermionic particles is also treated and a general computational formulation of this problem is given. For pedagogical purposes, the two-particle case is presented and the numerical dispersion of the simulated wave packets is compared with the analytical solutions.

KEY WORDS: Schroedinger wave equation, quantum computing, quantum lattice gas, quantum mechanics, computational physics

1 Introduction

Feynman's work regarding quantum mechanical computers used to simulate physical quantum mechanical behavior in a numerically efficient way [1, 2, 3] has subsequently led to several series of research papers concerned with a variety of details involving the particular quantum algorithm that best represents the Feynman path integral [4, 5]. The quantum algorithmic approach is based on a two-component complex field defined on a discrete spacetime lattice where unitary matrices act locally on the field causing its temporal evolution in discrete time steps. Using such a spatially discrete field makes it possible to computationally represent, in the long wavelength limit of modes in the discrete system, the dynamical time-dependent evolution of a continuous wave function in a manner that is numerically efficient.

In 1994 Bialynicki-Birula presented a general quantum algoithmic approach of this kind for modeling the Weyl, Dirac, and Maxwell equations on a body-centered cubic lattice in three-dimensions [6]. In a series of papers on simulating the one-dimensional Dirac equation [7, 8, 9], Meyer presented a quantum algorithm similar to that of Bialynicki-Birula with a variety of numerical simulations including the effects of boundary conditions, inhomogeneities, and an external scalar potential. Meyer set the quantum algorithm for the discretized path integral in the context of what is called the *quantum lattice gas method* and his algorithm is equivalent to the one-dimensional version of the Bialynicki-Birula quantum algorithm for the Dirac equation.

Contemporaneously with Meyer, two other series of papers on quantum lattice-gas models of the one-dimensional non-relativistic Schroedinger wave equation were presented by Succi and Benzi [10, 11] and by

*This work is supported by the Air Force Office of Scientific Research under the Quantum Computation for Physical Modeling initiative.

Boghosian and Taylor [12, 13, 14]. The approach taken by Succi and Benzi is somewhat more computationally oriented in that they begin with a "kinetic" lattice Boltzmann equation of motion[1] (effectively the one-dimensional Dirac equation in the Majorana representation) and show that the Schroedinger wave equation emerges as the governing equation of motion for the slow mode in the long wavelength "hydrodynamic" limit. That is, Succi and Benzi observed that the "macroscopic scale" Schroedinger wave equation arises from the "mesoscopic scale" Dirac equation in a manner quite analogous to how the macroscopic Navier-Stokes hydrodynamic fluid equation arises from the mesoscopic kinetic Boltzmann equation through the Chapman-Enskog expansion.

Boghosian and Taylor's approach follows more along the lines of Meyer's approach in that their model is developed as a generalization of the classical lattice gas method. A kinetic transport equation, now formuated directly at the "microscopic scale," again leds to the Schroedinger wave equation in the continuum limit. The Boghosian and Taylor quantum lattice gas model focuses on solving the many-body Schroedinger wave equation with an arbitrary scalar potential in an arbitrary number of spatial dimensions. They analytically argue for an exponential numerical speedup arising from simulation in the many-body sector of the full Hilbert space carried out simultaneously using quantum superposition of states. The Boghosian and Taylor version of the quantum algorithm is also cast explicitly for direct implementation of an array of quantum bits [13]. Polley has recently presented an argument for adding both an external scalar and vector potential into a quantum lattice-gas model by analytically demonstrating the discrete model's invariance with respect to a general local gauge transformation [18].

A characteristic feature of all these quantum algorithms, used to model the dynamical behavior of either relativistic or non-relativistic quantum particles, is that the governing wave function is well approximated as one approaches the continuum limit where the grid resolution of the spatial lattice become infinite (the lattice cell size approaches zero). Therefore, from the point-of-view of the modeler, there exists a "microscopic scale" where the unitary dynamical rules are locally applied in a discretized fashion and time advances forward in incremental units in a way that is quite artificial. Yet at the "macroscopic scale," which corresponds to the long wavelength limit of the dynamical modes in the discrete system, there is an emergent effective field theory for a complex amplitude field, continuous and differentiable in both space and time, that exactly obeys the physical quantum mechanical equations of motion. At the small scale (characterized by the lattice cell size) one imagines a system of fermionic particles undergoing local collisions and translation to nearby nodes of the lattice. Each of these fermionic particles occupies a local positional state at a specific lattice node with a certain probability amplitude. All the possible locations of the actual physical quantum particle are effectively modeled by the interfering set of probability amplitudes associated with this system of fermionic particles. That is, all the possible pathways are modeled simultaneously using a kind of kinetic system of locally interacting fermions on the small scale.

Seen as a kinetic system then, we may expect that there exists a *local equilibrium configuration of particles*. We require that this configuration be an eigenket, with unity eigenvalue, of the local unitary collision operator that is uniformly and spatially homogeneously applied to the lattice-based two-component field. Then the dynamical lattice-based system on all lattice nodes undergoes local relaxation towards this equilibrium configuration. However, unlike a classical kinetic system, the global configuration of particles does not relax to a single steady-state equilibrium. Instead, there are many steady-state global equilibrium configurations which effectively are the energy eigenstates of the "macroscopic scale" quantum mechanical equation of motion modeled by the quantum lattice gas. If the quantum lattice gas system is initialized in any one of the energy eigenstate global configurations, the macroscopic scale configuration of the system will remain fixed in time albeit the microscopic configuration of particles would be continually changing at every unit time step.[2] In the end, the Feynman path integral is efficiently and accurately recast as a kinetic dynamical process computed in parallel efficiently on a spacetime lattice.

In this paper we do not argure that the quantum lattice gas dynamical rules represent a local hidden variable theory of quantum mechanics. Although fundamental arguments can be made to limit the possible form of the local unitary operator in the quantum lattice gas [6, 7], these arguments lead to an algorithm suited for implementation on a quantum com-

[1] The classical lattice Boltzmann equation was popularized with its application to computational fluid dynamics [15, 16, 17].

[2] Given a finite size lattice used for modeling purposes, each local configuration oscillates in time even when the global configuration is a time-independent energy eigenvalue. However, the amplitude of the oscillation does approach zero as the lattice size becomes infinite.

puter. In our investigation of a suitable local unitary collision operator we have found that one quantum gate in particular, the square-root-of-swap given below in Section 2.3, is especially useful for modeling the Schroedinger wave equation in that the local equilibrium configuration discussed above is an eigenket of this gate and with unity eigenvalue. Therefore, we have selected the square-root-of-swap gate as our basic model quantum gate. As demonstrated in Section 2.6, we find that this quantum gate leads to an overall modeling error that is second-order in the temporal discretization and fourth-order in the spatial discretization. Another point regarding this particular gate is that when measurements are periodically made of the state of qubits in the system, which destroys quantum superpositions and entanglements in the system, the macroscopic scale behavior of the quantum lattice gas system is governed by the classical diffusion equation [19].

This paper is organized as follows. First, in Section 2 we describe the basic quantum algorithm, in particular, how we encode the wave function, how we use two basic quantum gates applied to the qubits at the nodes of the lattice. We first describe the algorithm using matrices and then we describe an equivalent finite difference formulation. Using the microscopic finite difference equations, we then derive the effective field theory at the macroscopic scale where both the lattice cell size and the update time step approach zero. Diffusive ordering holds, as is typical for lattice gas systems, where small-scale temporal fluctuations in the wave function go as the square of the magnitude of the small-scale spatial fluctuations. To confirm that our derivation is correct and to test the validity of the quantum lattice gas model, we test the time-dependent dispersion of a free Gaussian packet. We also test the system when it is initialized in an energy state, which is a fixed macroscopic scale steady-state configuration. We find that as we halve the lattice cell size (double the spatial resolution), the cumulative error in the model drops by a factor $2^{5.45} = 43.7$.

Second, in Section 3 we show how an external scalar potential may be modeled in the quantum lattice gas system by inducing a local phase rotation in the qubits at each node of the lattice. The qubits at a lattice node are phase rotated by an amount corresponding to the strength of the spatially dependent external potential at that node. We show how this local phase rotation, a kind of gauge transformation, produces an additional potential energy term in the Schroedinger wave equation. We then test the quantum algorithm against two well-known cases of harmonic oscillation in a parabolic potential well and quantum scattering off of and tunneling through a constant potential energy barrier. In both cases, the model behaves as expected.

Third, in Section 4 we test how well the quantum lattice gas can simulate the simultaneous dispersion of two fermionic particles. In the case of multiple particles, the operational quantum gate sequence to handle the many-body case is identical to the single particle case presented in Section 2. Therefore, the implementation of either situation on a quantum computer would be identical as well, except for state-preparation and measurements. However, since at present no quantum computer exists that can test the algorithm presented here, we are forced to consider the implementation on a classical computer and here the implementation for a many-body problem is much more complex than for the single-body problem. Nevertheless, we present a general formulation of the quantum gates in a second quantized representation where the basic computational operations are creation and annihilation of local particle occupancies. The advantage of such an implementation is that it is straightforward to implement the fundamental creation and annihilation operation is a way that respects the anti-commutation relations for fermionic particles. We demonstrate that the macroscopic scale behavior of the quantum lattice gas agrees with the exact time-dependent solution of the two-body wave equation.

Finally, we conclude this paper with a short description of results and share some lessons we learned after using the quantum lattice gas model extensively. We also point out some future directions that may be taken to expand the usefulness of the model.

2 Quantum Algorithm for a Single Free Particle

We describe the quantum lattice-gas algorithm for modeling the Schroedinger wave equation by considering the simplest case of a single free particle in a one-dimensional space. In this simple case, the wave function $\psi(x,t)$ obeys the following partial differential equation in the position representation

$$i\hbar\frac{\partial\psi(x,t)}{\partial t} = -\frac{\hbar^2}{2m}\frac{\partial^2\psi(x,t)}{\partial x^2}, \qquad (1)$$

where $\hbar$ is Planck's constant and m is the mass of the quantum particle. Here $\psi(x,t)$ is a continuous probability amplitude field (e.g. a continuous complex field).

2.1 Encoding the Wave Function

To "program" a quantum computer to simulate (1), it is necessary to first formulate an encoding scheme where a collection of qubits is used to store the value of the wave function. Since the number of qubits in any quantum computer is necessarily a finite number, the wave function will have to be approximated in the usual way by discretizing a physically continuous amplitude field into an artificially discrete and finite set of complex numbers. To do this, let us begin with a one-dimensional spatial lattice with L number of nodes. With each node of the lattice we associate a position basis ket denoted by $|x_l\rangle$, where $0 \geq l \geq L-1$. The discretized system ket in the position basis is

$$|\psi\rangle = \sum_{l=0}^{L-1} c_l |x_l\rangle, \tag{2}$$

where $c_l = \langle x_l|\psi\rangle$ is a complex number. In other words, the basic approach to model the single particle wave function governed by (1) is to express $|\psi\rangle$ as a sum of all the possible ways the particle can be situated on the lattice with a probability amplitude c_l associated with each possible location $|x_l\rangle$.

In our model, we assign two qubits to each node of the lattice, for a total of $2L$ qubits in the whole quantum computer. The qubits that reside at the lth node of the lattice are denoted by $|q_0^l\rangle$ and $|q_1^l\rangle$ and they are used to encode the coefficient c_l of (2) of the position ket for that node. Each qubit is a two-level quantum system $|q_a^l\rangle = \alpha_a^l|0\rangle + \beta_a^l|1\rangle$, where $|\alpha_a^l|^2 + |\beta_a^l|^2 = 1$ for $a = 0$ or 1 and $0 \geq l \geq L-1$. We consider each qubit to be a container that may or may not be occupied by the quantum particle. The quantum particle is said to *occupy* the ath local state at position x_l when $\beta_a^l = 1$. Similarly, the ath local state at position x_l is said to be *empty* when $\beta_a^1 = 0$.

To see how the qubit encoding works, we write $|\psi\rangle$ in the number representation. In the number representation, each basis state is expressible as the ket $|n_0^0 n_1^0 n_0^1 n_1^1 n_0^2 n_1^2 \cdots n_0^L n_1^L\rangle$, where $n_a^l = 0$ or 1 for all l and a. The Boolean variables n_a^l are called the *number variables* and they correspond to a binary indexing of the basis states in the number representation. Since we are concerned with modeling the one-particle wave equation, we need consider only a subset of all the basis states where only one of the number variables is 1 and all the rest are 0. This subset of all the basis states is called the *one-particle sector*. There are $2L$ such combinations and we shall label these with the binary encoding formula $|2^{2l+a}\rangle$, for $a = 0, 1$ and $0 \geq l \geq L-1$. Therefore, the system ket in the number representation can be written as

$$|\psi\rangle = \sum_{l=0}^{L-1} \sum_{a=0}^{1} \xi_{2l+a} |2^{2l+a}\rangle, \tag{3}$$

where each ξ_{2l+a} is a probability amplitude (e.g. complex number).

Now for each position ket $|x_l\rangle$ there are two corresponding basis states in the number representation $|2^{2l}\rangle$ and $|2^{2l+1}\rangle$. There are two *interfering possibilities* for a particle to occupy the lth position on the lattice. Therefore, the occupancy probability of the lth node is computed by first summing the probability amplitudes of these corresponding basis states and then computing the square of the absolute value thereof. In other words, the coefficient c_l in (2) is set equal to the sum of the on-site coefficients in (3)

$$c_l \equiv \xi_{2l} + \xi_{2l+1}. \tag{4}$$

The definition (4) is an essential part of the quantum lattice-gas model presented in this paper. In the section below, where we analytically predict an effective field theory for our artificially discretized model, we explain why we need to make this assignment. We will find that (4) is needed for the predicted effective field theory to accurately approximate the Schroedinger wave equation in the long-wavelength limit, which is also defined below.

2.2 Formulating a Suitable Gate Sequence

We shall require that the algorithmic scheme be at least second order convergent in space, so that as we double the grid resolution (e.g. double the number of qubits) we in turn reduce the numerical error due to the field discretization by a factor of one-quarter. With this type of convergence characteristic, we are assured that we can simulate a wave function governed by the Schroedinger wave equation (1) to any arbitrary degree of accuracy. After we formulate our algorithmic scheme, we will then a posteriori verify by direct numerical simulation that it is indeed at least a second-order convergent numerical scheme. In fact in Section 2.6 we will find that our numerical scheme is fourth-order convergent with an error that goes as $(\delta x)^4$.

To simulate the quantum behavior of the wave function, we seek to develop a sequence of 2-qubit gate operations that will act on a large collection of qubits in the simplest way. We impose the following four simplifying constraints:

1. All quantum gate operations are homogeneous and independent of space and time.

2. Only a single quantum gate is used to evolve the wave function and this gate is applied to each lattice node independently (locality).

3. To provide communication channels between lattice nodes, only the simplest gate is used (e.g. a swap gate).

4. Because the final value of the computed wave function depends on summing interfering possibilities according to (4), we shall use the Haddamard gate at the very end of the simulation prior to making a measurement of the wave function so that a single qubit at each node will encode the probability amplitude $c_l = \langle x_l|\psi\rangle$ in (2).

With two qubits per node, there are four on-site basis kets, $|0\rangle\otimes|0\rangle \equiv (1,0,0,0)$, $|0\rangle\otimes|1\rangle \equiv (0,1,0,0)$, $|1\rangle\otimes|0\rangle \equiv (0,0,1,0)$, and $|1\rangle\otimes|1\rangle \equiv (0,0,0,1)$. In the context of a quantum lattice-gas model, the unitary matrix $\hat{U}$ is called the *local collision operator* and the on-site ket $|\nu\rangle \equiv |0\rangle\otimes|1\rangle+|1\rangle\otimes|0\rangle = (0,1,1,0)$ is called the *number density ket.* To have a well behaved local equilibrium associated with the collision process, the local collision operator must have the number density ket as an eigenvector with unity eigenvalue.

2.3 Matrix Representation

The quantum gate that we use to evolve the wave function, which is applied independently on a site-by-site basis, is the square-root-of-swap gate

$$\hat{U} = \begin{pmatrix} 1 & 0 & 0 & 0 \\ 0 & \frac{1}{2}-\frac{i}{2} & \frac{1}{2}+\frac{i}{2} & 0 \\ 0 & \frac{1}{2}+\frac{i}{2} & \frac{1}{2}-\frac{i}{2} & 0 \\ 0 & 0 & 0 & -1 \end{pmatrix}. \tag{5}$$

The reason for calling this the square-root-of-swap gate is that $\hat{U}^2$ is the swap gate itself

$$\hat{U}\cdot\hat{U} = \begin{pmatrix} 1 & 0 & 0 & 0 \\ 0 & 0 & 1 & 0 \\ 0 & 1 & 0 & 0 \\ 0 & 0 & 0 & 1 \end{pmatrix}. \tag{6}$$

The two nontrivial eigenvalues of $\hat{U}$ are $\lambda_1 = 1$ and $\lambda_2 = -i$, with eigenvectors $|\nu_1\rangle = (0,1,1,0)$ and $|\nu_2\rangle = (0,-1,1,0)$, respectively. Also, since (5) causes mixing only between the single-particle basis kets $|0\rangle\otimes|1\rangle$ and $|1\rangle\otimes|0\rangle$, it conserves particle number. So (5) is an appropriate choice for the local collision operator.

The full collision operator, denoted $\hat{C}$, which acts on the system ket $|\psi\rangle$ is formed by a L-fold tensor product over the local collision operators $\hat{U}$ applied homogenously and independently on each node of the lattice

$$\hat{C} = \bigotimes_{l=0}^{L-1} \hat{U}. \tag{7}$$

Let us denote the swap operator by $\hat{\chi}_{\mu,\nu}$, where μ and ν index any two qubits in the system. The streaming operator, denoted $\hat{S}_1$, causes a global shift to the right of the first qubit on all the lattice nodes. Therefore, $\hat{S}_1$ can be represented by a sequence of swap operators acting on nearest neighbors

$$\hat{S}_1 = \prod_{l=0}^{\frac{L-1}{2}} \hat{\chi}_{2l,2l+2}. \tag{8}$$

In matrix form, $\hat{\chi}$ is a $2^2 \times 2^2$ permutation matrix

$$\hat{\chi} = \begin{pmatrix} 1 & 0 & 0 & 0 \\ 0 & 0 & 1 & 0 \\ 0 & 1 & 0 & 0 \\ 0 & 0 & 0 & -1 \end{pmatrix}. \tag{9}$$

The algorithm we use to model the Schroedinger wave equation involves multiple applications of the collision operator interleaved with streaming operations as follows:

$$|\psi(t+\tau/2)\rangle = \hat{E}_1^{\frac{1}{2}}|\psi(t)\rangle, \tag{10}$$

where the square root of the evolution operator is

$$\hat{E}_1^{\frac{1}{2}} = \hat{S}_1^{\mathrm{T}}\hat{C}\hat{S}_1\hat{C}. \tag{11}$$

Here $\hat{S}_1^{\mathrm{T}}$ denotes the transpose of $\hat{S}_1$ and is the inverse of $\hat{S}_1$. Application of $\hat{S}_1^{\mathrm{T}}$ causes a global shift to the left of the first qubit on all the lattice nodes. One full time step of the evolution is

$$|\psi(t+\tau)\rangle = \hat{E}_1|\psi(t)\rangle. \tag{12}$$

We use four applications of the collision operator in $\hat{E}_1$ because $\hat{C}^4$ is the identity operation. Note that $\hat{S}_1$ and $\hat{C}$ do not commute, otherwise (12) would be a trivial evolution equation.

Note that in (12), our choice of streaming the first qubit was arbitrary. A more balanced algorithmic approach would treat both qubits identically. Therefore, we could alternatively define one full time step as

$$|\psi(t+\tau)\rangle \equiv \hat{E}_2\hat{E}_1|\psi(t)\rangle, \tag{13}$$

where

$$\hat{E}_2^{\frac{1}{2}} = \hat{S}_2^{\mathrm{T}}\hat{C}\hat{S}_2\hat{C}, \tag{14}$$

and where the streaming operator $\hat{S}_2$ causes a global shift to the right of the second qubit on all the lattice nodes. The advantage of using the balanced algorithm (13) is that its error is fourth-order in space whereas for the unbalanced algorithm (12) it is only third-order.

2.4 Finite Difference Formulation

It is possible to specify the quantum algorithm to model the Schroedinger equation without the use of matrices. Instead we can write down a set of finite difference equations, which are equivalent to (10), but perhaps simpler to comprehend at first glance. To do this, let us introduce a new notation for the $2L$ probabilities amplitudes ξ_{2l+a} in (3). We will denote the two complex numbers per lattice node by $\varphi_0(x_l, t_n)$ and $\varphi_1(x_l, t_n)$. That is, we have L-pairs of complex numbers. Then, the quantum algorithmic operations (14) can be expressed as follows:

$$\text{if } \mathrm{mod}(n,4) = 0 \qquad (15)$$
$$\begin{aligned} \varphi_0(x_l,t_n) &= A^*\varphi_0(x_l,t_{n-1}) + A\varphi_1(x_l,t_{n-1}) \\ \varphi_1(x_l,t_n) &= A\varphi_0(x_l,t_{n-1}) + A^*\varphi_1(x_l,t_{n-1}), \end{aligned}$$
$$\text{if } \mathrm{mod}(n,4) = 1 \qquad (16)$$
$$\begin{aligned} \varphi_0(x_l,t_n) &= \varphi_0(x_{l-1},t_{n-1}) \\ \varphi_1(x_l,t_n) &= \varphi_1(x_l,t_{n-1}), \end{aligned}$$
$$\text{if } \mathrm{mod}(n,4) = 2 \qquad (17)$$
$$\begin{aligned} \varphi_0(x_l,t_n) &= A^*\varphi_0(x_l,t_{n-1}) + A\varphi_1(x_l,t_{n-1}) \\ \varphi_1(x_l,t_n) &= A\varphi_0(x_l,t_{n-1}) + A^*\varphi_1(x_l,t_{n-1}), \end{aligned}$$
$$\text{and if } \mathrm{mod}(n,4) = 3 \qquad (18)$$
$$\begin{aligned} \varphi_0(x_l,t_n) &= \varphi_0(x_{l+1},t_{n-1}) \\ \varphi_1(x_l,t_n) &= \varphi_1(x_l,t_{n-1}), \end{aligned}$$

where $A = \frac{1}{2} + \frac{i}{2}$. The finite-difference equation pair (15) is equivalent to the local collision operation $\hat{C}$, as is the pair (17). The equation pairs (16) and (18) are equivalent to the streaming operations $\hat{S}$ and $\hat{S}^{\mathrm{T}}$, respectively.[3]

This finite-difference representation of the algorithm is nearly identical to that presented by Boghosian and Taylor in 1997 [14] where the two on-site qubits are simultaneously streamed to the left and right after collision operation

$$\begin{aligned} \varphi_0(x_{l+1},t_n) &= A^*\varphi_0(x_l,t_{n-1}) - A\varphi_1(x_l,t_{n-1}) \\ \varphi_1(x_{l-1},t_n) &= -A\varphi_0(x_l,t_{n-1}) + A^*\varphi_1(x_l,t_{n-1}). \end{aligned} \qquad (19)$$

They noted that after four time steps, the total amplitude $\psi(x_l, t_n) = \phi_0(x_l, t_n) + \phi_1(x_l, t_n)$ satisfies a finite-difference equation which approximates the Schroedinger equation in the continuum limit. The two essential differences between the improved algorithm (15) through (18) presented in this paper and the quantum algorithm (19) appearing in [20] is that we have alleviated the problem of the occurrence of two non-interpenetrating lattice-gas systems independently evolving on different checker-board sub-lattices and we have doubled the numerical accuracy. This is a problem that occurs when both on-site qubits are simultaneously streamed because streaming only a single qubit at a time, as was done for the quantum lattice-gas model of the diffusion equation [19], causes interactions between all the qubits at each time step.

2.5 The Governing Partial Differential Equation

It is straightforward using a symbolic mathematics program, and tedious by hand, to use the update rules (15) through (18) to algebraically determine the value of φ_0 and φ_1 at a later time. With the initial wave function set at t_0, one complete cycle of the algorithm is completed at t_8 (that is, $t_8 - t_0 \equiv \delta\tau$). With the wave function defined as $\psi(x_l, t_n) \equiv \varphi_0(x_l, t_n) + \varphi_1(x_l, t_n)$, the result after one cycle is[4]

$$\begin{aligned} \psi(x_l,t_8) &= -\frac{1+i}{2}\psi(x_l,t_0) + \psi(x_{l+1},t_0) + \psi(x_{l-1},t_0) \\ &\quad -\frac{1-i}{4}\left[\psi(x_{l+2},t_0) + \psi(x_{l-2},t_0)\right], \end{aligned} \qquad (20)$$

Note that (20) is the simplified form of the finite-difference equation at the macroscopic scale when the system is very close to local equilibrium throughout the course of the evolution as $\varphi_0(x,t) = \varphi_1(x,t) \simeq \frac{1}{2}\psi(x,t)$ for all x. The full finite-difference equation is too long to present here, but is given in Appendix A. This result is a finite-difference equation for the fol-

[3] Noting that $A + A^* = 1$, this set of finite difference equations can be expressed in a more compact way

$$\begin{aligned} \varphi_0(x_{l+\epsilon},t_{n+1}) &= \varphi_0(x_l,t_n) + \Omega_0 \\ \varphi_1(x_l,t_{n+1}) &= \varphi_1(x_l,t_n) + \Omega_1 \end{aligned}$$

where $\epsilon = (-1)^n$ and $\Omega_0 = A(\varphi_1 - \varphi_0)$ and $\Omega_1 = -\Omega_0$, which has the standard form of a lattice-gas transport equation.

[4] Note that the result (20) is accurate up to fourth order in δx only in the situation where the initial system is in local equilibrium defined by $\varphi_0(x_l, t_n) = \varphi_1(x_l, t_n)$. In the more general situation when the system is not in local equilibrium where $\varphi_0(x_l, t_n) \neq \varphi_1(x_l, t_n)$, the result (20) is accurate only up to third order in δx.

lowing partial differential equation governing the continuous amplitude field $\psi(x,t)$

$$\frac{\partial\psi(x,t)}{\partial t} + \mathcal{O}(\delta t^2) = \frac{i}{2}\frac{\delta x^2}{\delta\tau}\frac{\partial^2\psi(x,t)}{\partial x^2} + \mathcal{O}(\delta x^4), \quad (21)$$

which is an approximation of (1) where the diffusion constant is $\hbar/m = \delta x^2/\delta\tau$ and where δx is the lattice cell size.

If one adds a phase angle ζ to the off-diagonal components of collision operator (5) to obtain a slightly more general collision operator

$$\hat{U} = \begin{pmatrix} 1 & 0 & 0 & 0 \\ 0 & \frac{1}{2}-\frac{i}{2} & \left(\frac{1}{2}+\frac{i}{2}\right)e^{i\zeta} & 0 \\ 0 & \left(\frac{1}{2}+\frac{i}{2}\right)e^{-i\zeta} & \frac{1}{2}-\frac{i}{2} & 0 \\ 0 & 0 & 0 & -1 \end{pmatrix}, \quad (22)$$

then the resulting governing partial differential equation will have its transport coefficient dependent on this phase angle as follows:

$$\frac{\partial\psi(x,t)}{\partial t} + \mathcal{O}(\delta t^2) = \frac{i}{2\sec\zeta}\frac{\delta x^2}{\delta\tau}\frac{\partial^2\psi(x,t)}{\partial x^2} + \mathcal{O}(\delta x^4). \quad (23)$$

This allows us to simulate a quantum system where a particle's mass can be arbitrarily large $m = \sec\zeta$, but has a minimum of one. Note that in this case the error is cubic and is proportional to $\sin\zeta$. So for very large masses, the accuracy of the model is reduced to third-order in space. Note that (23) is is valid effectively field theory at the macroscopic scale when the system is very close to local equilibrium where $\varphi_0(x,t) = \varphi_1(x,t) \simeq \frac{1}{2}\psi(x,t)$ for all x.

2.6 Numerical Confirmations

To numerically test that the quantum algorithm (12) is indeed equivalent to the finite-difference equation (20) and to see just how good of an approximation of the single-particle Schroedinger equation it is, we have preformed two simulations.

In the first simulation, we test the numerical time evolution of a Gaussian packet

$$\psi(x,0) = \frac{1}{\sigma^{\frac{1}{2}}\pi^{\frac{1}{4}}}e^{-\frac{x^2}{2\sigma^2}}, \quad (24)$$

where $\ell \geq x \geq L$ for a lattice of size $L = 64\ell$ and where the packet width is $\sigma = L/10$ as shown in Figure 1.

The exact anaytical solution of (21) is obtained by computing the Fourier components of the energy basis functions

$$a_o = \frac{1}{L}\int_{-L/2}^{L/2}\psi(x,0)dx \quad (25)$$

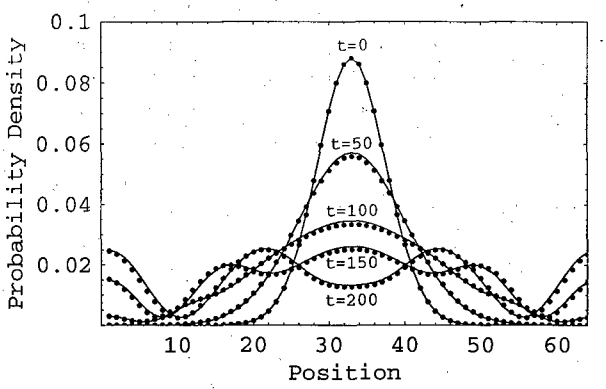

Figure 1: Time evolution of a Gaussian packet for a single quantum particle overplotted in succession where the x-axis is the position on a 64-node lattice in units of the lattice spacing ℓ and the y-axis is the probability density $|\psi(x,t)|^2$. The solid curves are the exact analytical solution and the circles are the data from the quantum lattice-gas simulation (the initial wave function was normalized, therefore the area under each curve is one). The lattice size is $L = 64\ell$. The initial Gaussian packet of with $\sigma = L/10$ at $t = 0$ is centered at $x = 32\ell$ and the dispersion is evident by observing the wave function at the subsequent times $t = 50\tau, 100\tau, 150\tau$, and 200τ. Periodic boundary conditions were used and $n_{\max} = 20$ energy eigenmodes were used to generate the exact solutions. A time scale factor $t_s = 1.04$ was used to improve the agreement between the numerical and analytical solutions.

$$a_n = \frac{2}{L}\int_{-L/2}^{L/2}\psi(x,0)\cos\left(2n\pi\frac{x}{L}\right)dx. \quad (26)$$

With $\hbar = 1$ and $m = 1$, the energy eigenvalues are

$$E_n = \frac{2n^2\pi^2\delta x^2}{L^2\delta t}, \quad (27)$$

and the time-dependent solution to (21) plotted in Figure 1 is

$$\psi_{\text{exact}}(x,t) = a_o + \sum_{n=1}^{n_{\max}} a_n \cos\left(2n\pi\frac{x}{L}\right)e^{-iE_nt/t_s}. \quad (28)$$

Note that in (28), time is scaled by a factor t_s to account for kinetic corrections to the time step. As the number of lattice nodes becomes large, this scaling factor approaches one.

The second test of the quantum lattice-gas algorithm as a model of the Schroedinger wave equation is the measurement of its numerical convergence. Multiple simulations (10 in total) were carried out for lattice sizes ranging from $L = 8\ell, 16\ell, 32\ell, \ldots$ up to $L = 8192\ell$. In each case the initial state of the simulation was the ground state (a sinusoidal energy eigen-

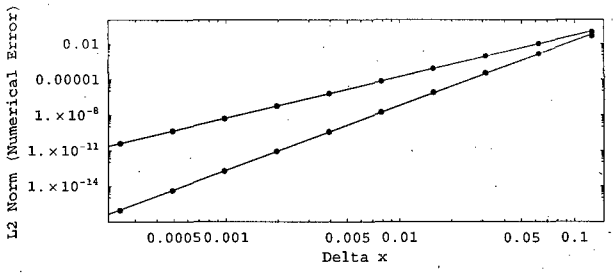

Figure 2: Log-log plot of the numerical error versus resolving grid cell size, δx, indicating the convergence property of the quantum lattice-gas algorithm (12) and (13) for the Schroedinger equation. The data (black circles) are taken from numerical simulations with grid sizes from $L = 8\ell$ up to 8192ℓ after a single time step $T = \tau$. The solid curves are best-fit linear regression with a slope of 3.48 and 5.45 for the models defined by (12) and (13), respectively. These results demonstrate third-order and fourth-order convergence in space for the two models, respectively.

state)

$$\psi(x,0) = \psi^{\text{exact}}(x) = \frac{\cos(2\pi x/L)}{\sqrt{L/2}}. \qquad (29)$$

Each simulation was run for one time step $T = \tau$ and the numerical error, denoted ϵ, from the exact solution was then measured using the following formula

$$\epsilon(L) = \frac{1}{L}\sqrt{\sum_{x=1}^{L}\{|\psi(x,T)|^2 - |\psi^{\text{exact}}(x)|^2\}^2}. \qquad (30)$$

We define the grid resolution as the inverse of the total number of lattice points. That is, for a box of size 1, the *resolving cell size* is defined as $\delta x \equiv \frac{1}{L}$. A plot of the error versus the resolution is given in Figure 2. As the resolution is increased, the error drops off as $\epsilon(L) \sim L^{-5.45}$.

3 Adding an External Scalar Potential

It is possible to model an external potential by applying a local phase change to the system wave function [13, 14]

$$\psi(x,t) \to e^{-iV(x)\delta t}\psi(x,t). \qquad (31)$$

The effect of this phase change is to alter the finite difference equation (20) as follows

$$\begin{aligned}\psi(x_l,t_8) &= -\frac{1+i}{2}e^{-iV(x_l)\delta t}\psi(x_l,t_0) \qquad (32)\\ &+ e^{-iV(x_{l+1})\delta t}\psi(x_{l+1},t_0)\\ &+ e^{-iV(x_{l-1})\delta t}\psi(x_{l-1},t_0)\\ &- \frac{1-i}{4}\left[e^{-iV(x_{l+2})\delta t}\psi(x_{l+2},t_0)\right.\\ &\left.+ e^{-iV(x_{l-2})\delta t}\psi(x_{l-2},t_0)\right].\end{aligned}$$

If we expand the potential terms in the arguments of the exponentials

$$V(x_{l+1})\delta t = V(x_l)\delta t + \delta t\delta x\left.\frac{dV(x)}{dx}\right|_{x=x_l} + \mathcal{O}(\delta t\delta x^2) \qquad (33)$$

we see that we can neglect the second term on the RHS because of diffusive ordering $\delta t\delta x \sim \delta x^3$ since we need to keep terms only to order δx^2. Therefore, in the continuum limit (32) is well approximated by

$$\begin{aligned}\psi(x_l,t_8) &= -\frac{1+i}{2}e^{-iV(x_l)\delta t}\psi(x_l,t_0) \qquad (34)\\ &+ e^{-iV(x_l)\delta t}\left[\psi(x_{l+1},t_0)+\psi(x_{l-1},t_0)\right]\\ &- \frac{1-i}{4}e^{-iV(x_l)\delta t}\left[\psi(x_{l+2},t_0)+\psi(x_{l-2},t_0)\right].\end{aligned}$$

Now multiplying through by $e^{iV(x_l)\delta t}$ and expanding the LHS to order δt^2 we have the following finite-difference equation:

$$\begin{aligned}[1+iV(x_l)\delta t]\,\psi(x_l,t_8) &= -\frac{1+i}{2}\psi(x_l,t_0) \qquad (35)\\ &+ \psi(x_{l+1},t_0)+\psi(x_{l-1},t_0)\\ &- \frac{1-i}{4}\left[\psi(x_{l+2},t_0)+\psi(x_{l-2},t_0)\right].\end{aligned}$$

In the continuum limit, this finite-difference equation represents the Schroedinger wave equation with an external potential term

$$\frac{\partial\psi(x,t)}{\partial t} + \mathcal{O}(\delta t^2) = \frac{i}{2}\frac{\delta x^2}{\delta\tau}\frac{\partial^2\psi(x,t)}{\partial x^2} - iV(x)\psi(x,t) + \mathcal{O}(\delta x^4). \qquad (36)$$

To confirm the validity of (36) we perform the following numerical simulations that yield results that can be checked against analytical predictions:

1. Harmonic oscillation of a displaced Gaussian wave packet in a parabolic potential.
2. Quantum tunneling through a potential barrier.

3.1 Harmonic Oscillator

The first numerical test presented here is the simulation of the behavior of a wave packet in an external parabolic potential. This is the well-known problem of

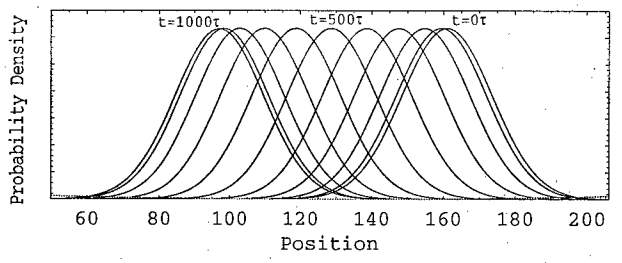

Figure 3: Time evolution of a Gaussian packet initially displaced by $a = 32\ell$ lattice sites from the center of a parabolic potential well with $K = 10^{-5}$. The width of the packet is $\alpha = 14.4\ell$. The time development of the Gaussian packets over plotted in succession where the x-axis is the position on a $L = 256\ell$ node lattice and the y-axis is the probability density $|\psi(x,t)|^2$. The red curve is the parabolic potential. The $\hbar = 1$ and $m = 1$, the time period of the oscillation is $T_c = \frac{2\pi}{\omega_c} = 1986.92\tau$. A total of ten profiles are over plotted corresponding to time $t = 0, 100\tau, 200\tau, ..., 1000\tau$, which is approximately half of the oscillation time period, so the packet is seen to "swing" to the other side of the potential well while maintaining a fixed shape as analytically predicted.

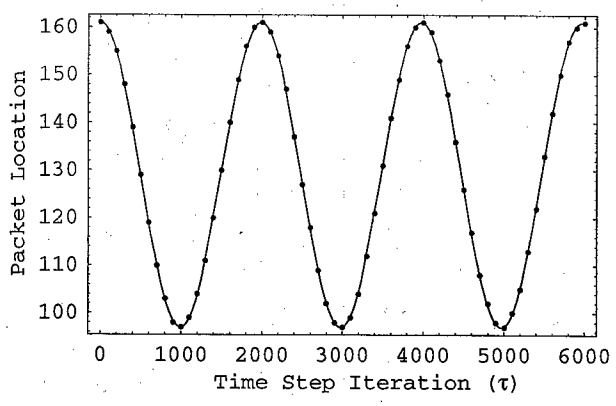

Figure 4: A comparison between the analytical and numerical predictions of the location of an oscillating Gaussian packet in a harmonic parabolic potential well. The solid curve is the analytical prediction and the black circles are the numerical data taken from the quantum lattice gas simulation presented in Figure 3. In the simulation, the packet is initially displaced 32 lattice units from the center of the grid at lattice node 128 for a periodic system with a total of $L = 256\ell$ nodes. The numerical predictions are in excellent agreement with the exact analytical solution.

the linear harmonic oscillator. Schroedinger analytically calculated the exact time-dependent solution for the evolution of a Gaussian packet that is displaced by a distance a from its central ground state in a parabolic potential well of the form $V(x) = \frac{1}{2}Kx^2$. The initial wave function is

$$\psi(x,0) = \frac{\alpha^{\frac{1}{2}}}{\pi^{\frac{1}{2}}} e^{-\frac{1}{2}\alpha^2(x-a)^2}, \qquad (37)$$

where $\alpha = \left(mK/\hbar^2\right)^{\frac{1}{4}}$ is the width of the packet and $\omega_c = (K/m)^{\frac{1}{2}}$ is the angular frequency of the classical harmonic oscillator [21]. The exact time-dependent solution for the probability density is the following:

$$|\psi(x,t)|^2 = \frac{\alpha}{\pi^{\frac{1}{2}}} e^{-\frac{1}{2}\alpha^2(x-a\cos\omega_c t)^2}. \qquad (38)$$

A derivation of the result (38) is also presented by Schiff [22].

To test the quantum lattice gas algorithm against (38) we used a periodic lattice with $L = 256\ell$ nodes. The initial Gaussian packet is displaced to the right of the center of the grid by 32 lattice nodes and so is initially located at $x_o = 160\ell$ as shown in Fig 3. With $\hbar = 1$ and $m = 1$, the classical time period is $T_c = 2\pi/\omega_c = 1987\tau$. So letting the simulation run for 1000 iterations allows the packet to the other side of the potential well near position $x = 96\ell$ as demonstrated in Fig 3.

The simulation was rum for a total of 6000 time steps and the location of the peak of the Gaussian wave packet was recorded every 100τ time steps. This data is plotted in Fig 4. The location of the peak oscillates in time as expected. Overplotted on this numerical data is the exact solution for the oscillation $a\cos\omega_c t + x_o$ and the agreement between the analytical solution and the numerical data is excellent.

3.2 Scattering Off A Potential Barrier

The next numerical test of the quantum lattice gas is to simulate the well-known case of quantum tunneling through a constant potential barrier of width a. That is, $V(x) = V_o$ for $0 \le x \le a$ and $V(x) = 0$ otherwise. The initial wave function is a Gaussian packet with net momentum to the right

$$\psi(x,0) = \frac{1}{\pi^{\frac{1}{4}}\sigma^{\frac{1}{4}}} e^{-\frac{1}{2}\left(\frac{x-x_o}{\sigma}\right)^2 + ipx}, \qquad (39)$$

where p is the momentum parameter. We choose the mean kinetic energy of the packet to be equal to the constant energy level of the potential barrier $\frac{1}{2}p^2 = V_o$. In this case, the packet tunnels through the barrier but the sum of the transmission and reflection probabilities are less than one because there is a resonance effect where the particle is also trapped inside of the barrier. This effect is observed in the numerical simulation shown in Figure 5.

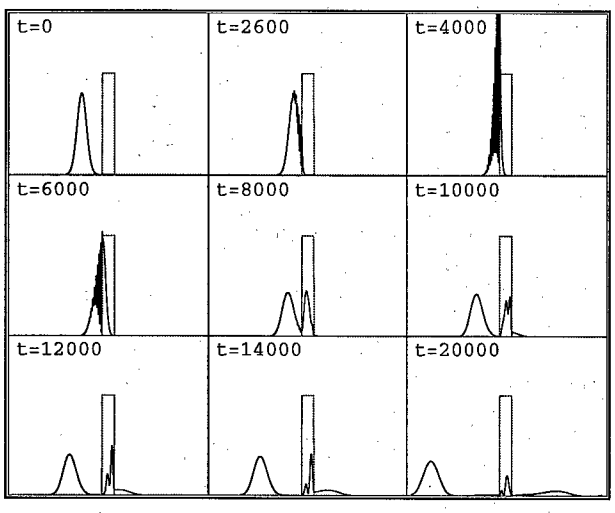

Figure 5: A sequence of snap shots of the time evolution of a packet that is incident from the left on to a potential barrier where the mean kinetic energy of the packet equals the energy of the barrier. The x-axis is the lattice position and the y-axis is the probability density. The iteration time step for each frame of the sequence is labeled in the upper left corners. The simulation was run on a periodic grid of size $L = 4000\ell$ for a total of 20000 time steps. The width of the incident packet was set to $\sigma = .035L = 140\ell$ and the initial momentum parameter was set to $p = 0.1$ in units where $\ell = 1$, $\tau = 1$ and $m = 1$. The width of the barrier was set to $a = 0.064L = 256\ell$. As expected the numerical simulation clearly demonstrates the resonance effect where there is a non-zero probability of the particle to be trapped within the barrier itself.

4 Two Fermionic Particles

The efficiency of the quantum algorithm (12) becomes evident when it is used to simulate the dynamics of multiple quantum particles. The case of multiple quantum particles is still handled by the same evolution operator $\hat{E}$ that we tested for the single particle case. The particular sequence and number of quantum gate operations remains fixed, independent of the number of particles to be simulated. The only difference is how the system wave function is initialized.

In this section, for pedagogical reasons, we will consider the case of simulating two free quantum particles. The approach we use in this case can be directly generalized to the many-particle case.

To begin with we write the Schroedinger wave equation for two free quantum particles

$$i\hbar\frac{\partial\psi(x,y,t)}{\partial t} = -\frac{\hbar^2}{2m}\frac{\partial^2\psi(x,y,t)}{\partial x^2} - \frac{\hbar^2}{2m}\frac{\partial^2\psi(x,y,t)}{\partial y^2}, \tag{40}$$

where x and y are the spatial coordinates of the first and second particle, respectively. Since the wave function is spatially separable as $\psi(x,y,t) = \varphi(x,t)\varphi(y,t)$, the analytical solution to (40) is obtained in a similar fashion to the one-body case by computing the Fourier components of the energy basis functions

$$a_o = \frac{1}{L}\int_{-L/2}^{L/2}\varphi(x,0)dx \tag{41}$$

$$a_n = \frac{2}{L}\int_{-L/2}^{L/2}\varphi(x,0)\cos\left(2n\pi\frac{x}{L}\right)dx \tag{42}$$

$$b_n = \frac{2}{L}\int_{-L/2}^{L/2}\varphi(x,0)\sin\left(2n\pi\frac{x}{L}\right)dx. \tag{43}$$

The energy eigenvalues are still given by (27) and the time-dependent single-particle solution is

$$\varphi(x,t) = a_o + \sum_{n=1}^{n_{\max}}\left[a_n\cos\left(2n\pi\frac{x}{L}\right) + b_n\sin\left(2n\pi\frac{x}{L}\right)\right]e^{-iE_nt/t_s}, \tag{44}$$

which is basically the same as (28) except that we had to add the sin term because with two particles the wavefunction is not even, as is (24) for example. We shall test the time evolution of two Gaussian packets. The initial wave function in our test is the odd function

$$\psi_{\text{exact}}(x,y,t) = \frac{1}{\sqrt{2}}[\varphi_{\alpha_1,\sigma_1}(x,t)\varphi_{\alpha_2,\sigma_2}(y,t) - \varphi_{\alpha_1,\sigma_1}(y,t)\varphi_{\alpha_2,\sigma_2}(x,t)], \tag{45}$$

where

$$\varphi_{\alpha,\sigma}(x,0) = \frac{1}{\sigma^{\frac{1}{2}}\pi^{\frac{1}{4}}} e^{-\frac{(x-\alpha)^2}{2\sigma^2}}. \quad (46)$$

The subscripts on the function $\varphi_{\alpha,\sigma}$ denote its dependence on the position and width of the individual Gaussian packet. This functional dependence is actually contained within the form of the coefficients a_o, a_n, and b_n that depend on the position and width of the Gaussian packet in accordance with (41) through (43). Note that given the form of (45), $\psi_{\text{exact}}(x,x,t) = 0$ which satisfies the Pauli exclusion principle.

4.1 Numerical Confirmation

To numerically simulate the evolution of the two-particle wave function governed by (40) using quantum algorithm (12) we must use a new computational formulation to implement our algorithm. The finite-difference equation implementation that we used in Section 2.4, in the single-particle case, cannot be directly applied in the two-particle case to each particle individually because it does not allow for the possibility when the particles are quantum mechanically entangled. In general, this will be the case when there is an interaction between the particles. Therefore, we shall use an implementation that can handle the most general situations involving correlated particles and one that naturally scales to handle an arbitrarily large number of particles in the system.

We shall represent the basic quantum gate operations in terms of the fermionic creation and annihilation operators in the number representation, denoted $\hat{a}_\alpha^\dagger$ and $\hat{a}_\alpha$ respectively, and use this approach as the basis for a general computational formulation applicable, in particular, to our algorithm and, in general, to any quantum algorithm. Acting on a system of Q qubits, $\hat{a}_\alpha^\dagger$ and $\hat{a}_\alpha$ create and destroy a particle occupancy encoded in the αth qubit

$$\hat{a}_\alpha^\dagger|n_1 \ldots n_\alpha \ldots n_Q\rangle = \begin{cases} 0 & , \ n_\alpha = 1 \\ |n_1 \ldots 1 \ldots n_Q\rangle & , \ n_\alpha = 0 \end{cases} \quad (47)$$

$$\hat{a}_\alpha|n_1 \ldots n_\alpha \ldots n_Q\rangle = \begin{cases} |n_1 \ldots 0 \ldots n_Q\rangle & , \ n_\alpha = 1 \\ 0 & , \ n_\alpha = 0 \end{cases}. \quad (48)$$

The fermionic creation and annihilation operators satisfy the anti-commutation relations

$$\begin{aligned} \{\hat{a}_\alpha, \hat{a}_\beta^\dagger\} &= \delta_{\alpha\beta} \quad (49) \\ \{\hat{a}_\alpha, \hat{a}_\beta\} &= 0 \\ \{\hat{a}_\alpha^\dagger, \hat{a}_\beta^\dagger\} &= 0. \end{aligned}$$

The number operator $\hat{n}_\alpha \equiv \hat{a}_\alpha^\dagger \hat{a}_\alpha$ has eigenvalues of 1 or 0 in the number representation when acting on a pure state, corresponding to the αth qubit being in state $|1\rangle$ or $|0\rangle$ respectively.

The square-root-of-swap gate (5) acting on the on-site qubits indexed by α and $\alpha+1$ can be expressed in terms of the creation and annihilation operators as

$$\begin{aligned} \hat{U}_{\alpha,\alpha+1} &= A^*\hat{n}_\alpha(\mathbf{1} - \hat{n}_{\alpha+1}) - A\hat{a}_\alpha^\dagger\hat{a}_{\alpha+1} - A\hat{a}_{\alpha+1}^\dagger\hat{a}_\alpha \\ &+ A^*(\mathbf{1} - \hat{n}_\alpha)\hat{n}_{\alpha+1} + \mathbf{1} - \hat{n}_\alpha - \hat{n}_{\alpha+1}, \quad (50) \end{aligned}$$

where $A = \frac{1}{2} + \frac{i}{2}$. Also, the swap operator (9) acting between the first qubits indexed by α and β at neighboring nodes can be expressed in terms of the creation and annihilation operators as

$$\hat{\chi}_{\alpha,\beta} = \mathbf{1} - \hat{a}_\alpha^\dagger\hat{a}_\beta - \hat{a}_\beta^\dagger\hat{a}_\alpha - \hat{n}_\alpha - \hat{n}_\beta. \quad (51)$$

The quantum gates (50) and (51) are used to implement the quantum lattice gas collision and streaming operations, respectively [23].

The basis state in the two-particle sector can be labeled with the binary encoding formula $|2^{\alpha-1}+2^{\beta-1}\rangle$ where the integers α and β are in the ranges $1 \le \alpha \le Q$ and $\alpha+1 \le \beta \le Q$. The number of basis states in this case is the binomial coefficient $\binom{Q}{2}$. The system ket can then be expressed in the two-particle sector as

$$|\psi\rangle = \sum_{\alpha=1}^{Q}\sum_{\beta=\alpha+1}^{Q} \xi_{\alpha,\beta}|2^{\alpha-1} + 2^{\beta-1}\rangle. \quad (52)$$

Since there are two qubits per site, we initialize the wave function using (45) as follows:

$$\xi_{\alpha,\beta} \equiv \psi_{\text{exact}}\left(\lfloor\frac{\alpha+1}{2}\rfloor - \frac{L+1}{2}, \lfloor\frac{\beta+1}{2}\rfloor - \frac{L+1}{2}, 0\right), \quad (53)$$

where the notation $\lfloor x \rfloor$ means the floor of x and where $Q \equiv 2L$. The floor operation is used so that the initial value of the wave function at each node is divided evenly between each pair of on-site qubits. This is on account of definition (4) that allowed us to have interfering possibilities for a single particle to occupy a single position on the lattice. Moreover in the two particle case, still only a single particle can occupy a single position because of the form of the wave function (45) which is consistent with the anti-commutater relations (49). However, particle one can interfere on-site with itself or with particle two, or vice versa since the particles are indistinguishable.

At this point we have described how we implement the two quantum gates used in our algorithm, how

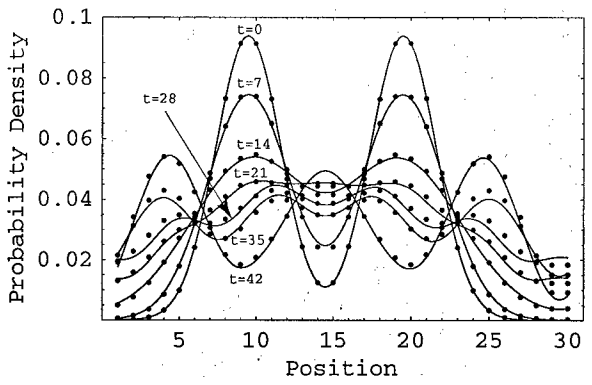

Figure 6: Time evolution of two fermionic particles initialized as Gaussian packets overplotted in succession where the x-axis is the position on a 30-node lattice in units of the lattice spacing ℓ and the y-axis is the probability density $|\psi(x_1, x_2, t)|^2$ projected onto the x_1-axis. The solid curves are the exact analytical solution and the circles are the data from the quantum lattice-gas simulation (the initial wave function was normalized, therefore the area under each curve is one). The initial Gaussian packets of width $\sigma = 3\ell$ at $t = 0$ of the first and second particle is centered at $x = 10\ell$ and $x = 20\ell$, respectively. The dispersion of both packets is evident by observing the wave function at the subsequent times $t = 7\tau, 21\tau, 28\tau, 35\tau$ and 42τ. Periodic boundary conditions were used and $n_{\max} = 40$ energy eigenmodes were used to generate the exact solutions at four times the resolution of the numerical solution. No time scale factor was used and there is good agreement between the analytical and numerical predictions at all later times of the numerical simulation as demonstated by the graphs.

we enumerate the basis states, and how we initialize the two-body wave function in this basis. The only remaining issue left to describe is how we project the two-coordinate wave function $\psi(x, y, t)$ on to a single-coordinate wave function $\psi(x, t)$ that can be plotted on a single physical axis. Because of the underlying lattice in our system this is straightforward to do by summing out one of the coordinates as follows:

$$\psi(x_l, t_n) \equiv \sum_{m=0}^{L-1} \psi(x_l, y_m, t_n). \qquad (54)$$

If $\psi(x_l, y_m, t_n)$ is normalized then so is $\psi(x_l, t_n)$ according to (54). A comparison of the time evolution of the analytical solution (45) and the numerical solution (54) for a lattice with 30 nodes is shown in Figure 6. Even with this small lattice, throughout the time evolution of the model run the numerical predictions are in good agreement with the predictions of the exact solution.

5 Conclusion

We have presented a quantum algorithm that is an efficient and accurate scheme for simulating the time-dependent evolution of a system of quantum particles governed by the non-relativistic Schroedinger wave equation. The scheme uses a quantum lattice gas system of particles colliding and hopping on a lattice. The algorithm is efficient in the sense that the computational effort needed to simulate an arbitrarily large number of particles (within the constraint of the grid resolution) exactly equals the computational work needed to simulate a single particle, given that the algorithm is executed on a quantum computer that remains phase-coherent throughout the entire coarse of the simulation. However, a limitation does exist on state preparation (*i.e.* initialize the quantum computer's memory) and we have not argued here that it is possible to initialize the many-body wave function in an efficient way. For that matter, have we also have not argued that it is possible to measure the final state (reading the quantum computer's memory) of the computed wave function in an efficient way. Nevertheless, the quantum algorithm presented here, which is a way of representing a discretized Feynman path integral, has the useful feature that it is explicit in time where the value of the wave function at location x and time $t+\tau$ depends only on the previous values of the wave function at time t in the immediate vicinity of x. Since the algorithm is unitary and fourth-order accurate in space, it is useful even for implementation on a classical computer.

We have carried out a variety of numerical tests proving that the quantum algorithm indeed allows us to faithfully reproduce the correct dynamical behavior of a continuous and differentiable wave function in the presence of an external potential. However, the total probability for finding the quantum particle in the system is not exactly conserved in this quantum lattice gas model. One must approach the continuum limit to achieve a high degree of probability conservation. Since we have demonstrated that the quantum lattice gas model is fourth-order convergent in space, it is always possible to choose a grid resolution that achieves the necessary fixed numerical accuracy required by any application.

We have also described and carried out the numerical simulation of two fermionic particles, which are non-interacting except for a quantum mechanical exchange force arising from the anti-commutation relations. The numerical formalism used to implement the quantum lattice gas algorithm represents the basic quantum gates in terms of quadratic products of cre-

ation and annihilation operators in a second quantized representation. This formalism straightforwardly handles an arbitrarily large number of particles. The simulation is carried out in the many-body sector (*i.e.* a Fock space where the number of particles is fixed) where all the basis states are enumerated by a simple binary encoding formula. In general, the wave function is initialized using a Slater determinant so that the Pauli exclusion principle is satisfied and the wave function is odd. In all the test cases (single free particle, single particle in an external potential, and two free fermions) the numerical predictions agreed extremely well the analytical predictions and exact solutions.

It is important to realize that it is possible to push the quantum lattice gas model into regimes where the numerically predicted results are absolutely wrong. This occurs when the local configurations are far from local equilibrium. Remember that local equilibrium exists on a lattice node when the qubits at that node have identical phase. Therefore, large gradients in the macroscopic profile of the modeled wave function may cause a large phase difference between the on-site qubits eventually resulting in anomalous large-scale behavior in the model. A good example of this occurs when the momentum of a moving wave packet is too high. In this case, since the real and imaginary parts of the wave function are sinusoidal, if the momentum is so high that the wavelength of the traveling wave is on the order of the lattice cell size ($\lambda = \hbar/p \sim \ell$), then after a few times step iterations of the algorithm, large phase differences in the on-site qubits occur. In this case, the local on-site configuration will not relax toward the correct local equilibrium. Fortunately, the norm of the modeled wave function will deviate from unity in these types of cases. Therefore, it is straightforward to test if the model predictions are non-physical by periodically checking the norm of the wave function.

Interaction potentials between particles can also be modeled using this quantum lattice gas method [14]. We still need to perform simulations of a many-body system with an interaction potential. Also, numerical tests in two and three dimensions should be conducted. In this case, it would be straightforward to test the addition of an external vector potential using the results analytically predicted by Polley [18]. The simulation of the dynamical behavior of the positronium atom would be a reasonable next step for the application of the quantum lattice gas method to quantum mechanical computational physics.

6 Acknowledgements

J. Yepez would like to thank George and Linda Vahala for their critical inspection of this quantum lattice-gas model and helpful discussions.

A Appendix

The full finite-difference equation for the quantum lattice-gas model presented in this paper is very long. To simplify this expression, we introduce a *local neighborhood vector* with the following 18 components

$$\begin{aligned}\vec{\eta}(x_l,t) &= (\varphi_0(x_l,t),\varphi_1(x_l,t), \\ &\quad \varphi_0(x_{l+1},t),\varphi_1(x_{l+1},t),\varphi_0(x_{l-1},t),\varphi_1(x_{l-1},t), \\ &\quad \varphi_0(x_{l+2},t),\varphi_1(x_{l+2},t),\varphi_0(x_{l-2},t),\varphi_1(x_{l-2},t), \\ &\quad \varphi_0(x_{l+3},t),\varphi_1(x_{l+3},t),\varphi_0(x_{l-3},t),\varphi_1(x_{l-3},t), \\ &\quad \varphi_0(x_{l+4},t),\varphi_1(x_{l+4},t),\varphi_0(x_{l-4},t),\varphi_1(x_{l-4},t)).\end{aligned} \tag{55}$$

We define the following two *coefficient vectors*

$$\begin{aligned}\vec{\alpha} &\equiv (-3,-3i,3,i,-3,-5i,1,i,3,3i,-1,i,1,3i,0,0,-1,-i) \\ \vec{\beta} &\equiv (-3i,-3,-5i,-3,i,3,3i,3,i,1,3i,1,i,-1,-i,-1,0,0).\end{aligned} \tag{56}$$

The microscopic evolution equation (13), explicitly written out, has the following protocol of operations

$$|\psi(t_{16})\rangle \equiv \left(\hat{S}_2^{\mathrm{T}}\hat{C}\hat{S}_2\hat{C}\hat{S}_2^{\mathrm{T}}\hat{C}\hat{S}_2\hat{C}\right)\left(\hat{S}_1^{\mathrm{T}}\hat{C}\hat{S}_1\hat{C}\hat{S}_1^{\mathrm{T}}\hat{C}\hat{S}_1\hat{C}\right)|\psi(t_0)\rangle. \tag{57}$$

The corresponding full finite-difference equation can be specified by the following dot product of these vectors

$$\varphi_0(x_l,t_{16}) = \frac{\vec{\alpha}\cdot\vec{\eta}(x_l,t_0)}{16} \tag{58}$$

$$\varphi_1(x_l,t_{16}) = \frac{\vec{\beta}\cdot\vec{\eta}(x_l,t_0)}{16}. \tag{59}$$

Note that if t_0 is the initial time, then the interval $\tau \equiv t_{16}$ is defined the update time step. The finite-difference equation for $\psi = \varphi_0 + \varphi_1$ is

$$\psi(x_l,t_{16}) = \frac{(\vec{\alpha}+\vec{\beta})\cdot\vec{\eta}(x_l,t_0)}{16} \tag{60}$$

and it has a high degree of numerical accuracy as indicated in Figure 2.

References

[1] Richard P. Feynman. Simulating physics with computers. *International Journal of Theoretical Physics*, 21(6/7):467–488, 1982. pages 1

[2] Richard P. Feynman. Quantum mechanical computers. *Optics News*, 11(2):11–20, 1985. pages 1

[3] Anthony J.G. Hey and Robin W. Allen, editors. *Feynman Lectures on Computation*. The Advanced Book Program. Addison-Wesley Publishing Company, Inc., 1996. pages 1

[4] Richard P. Feynman. Space-time approach to non-relativistic quantum mechanics. *Reviews of Modern Physics*, 20(2):367–387, 1948. pages 1

[5] Richard P. Feynman and A.R. Hibbs. *Quantum Mechanics and Path Integrals*. McGraw-Hill, 1965. pages 1

[6] Iwo Bialynicki-Birula. Weyl, dirac, and maxwell equations on a lattice as unitary cellular automata. *Physical Review D*, 49(12):6920–6927, 1994. pages 1, 2

[7] David A. Meyer. From quantum cellular automata to quantum lattice gas. *Journal of Statistical Physics*, 85(5,6):551–574, 1996. pages 1, 2

[8] David A. Meyer. Quantum mechanics of lattice gas automata: One-particle plane waves and potentials. *Physical Review E*, 55(5):5261–5269, 1997. pages 1

[9] David A. Meyer. Quantum mechanics of lattice gas automata ii. boundary conditions and other inhomogeneities. *Quant-Ph*, 9712052:1–24, 1997. pages 1

[10] Sauro Succi and R. Benzi. Lattice boltzmann equation for quantum mechanics. *Physica D*, 69:327–332, 1993. pages 1

[11] Sauro Succi. Numerical solution of the schrodinger equation using discrete kinetic theory. *Physical Review E*, 53(2):1969–1975, 1996. pages 1

[12] Bruce M. Boghosian and Washington Taylor IV. Quantum lattice gas models for the many-body schrodinger equation. *International Journal of Modern Physics C*, 8:705–716, 1997. pages 2

[13] Bruce M. Boghosian and Washington Taylor IV. Simulating quantum mechanics on a quantum computer. *Physica D*, 120:30–42, 1998. pages 2, 8

[14] Bruce M. Boghosian and Washington Taylor IV. A quantum lattice-gas model for the many-particle schrodinger equation in d dimensions. *Physical Review E*, 57:54–66, 1998. pages 2, 6, 8, 13

[15] S. Succi, R. Benzi, and F. Higuera. The lattice boltzmann equation: A new tool for computational fluid dynamics. *Physica D*, 47:219–230, 1991. pages 2

[16] Y.H. Qian, D. d'Humiéres, and P. Lallemand. Lattice bgk models for navier-stoke equation. *Europhysics Letters*, 17(6BIS):479–484, 1992. pages 2

[17] Hudong Chen, Shiyi Chen, and William H. Mattaeus. Recovery of the navier-stokes equations using a lattice-gas boltzmann method. *Physical Review A*, 45(8):R5339–R5342, 1992. pages 2

[18] Lutz Polley. Schrodinger equation as the universal continuum limit of nonrelativistic coherent hopping on a cubic spatial lattice. *Los Alamos National Laboratory Electronic Archive*, quant-ph/9811048:1–6, 2000. pages 2, 13

[19] Jeffrey Yepez. Quantum lattice-gas model for the diffusion equation. *International Journal of Modern Physics C*, 12(9):1–19, 2001. Presented at the 9th International Conference on Discrete Simulation of Fluid Dynamics, Santa Fe, NM, August 22, 2000. pages 3, 6

[20] Bruce M. Boghosian and Washington Taylor IV. A quantum lattice gas models for the many-body schrodinger equation. *LANL Archive*, quant-ph/9604035, 1996. pages 6

[21] Erwin Schrodinger. *Naturwiss*, 14:664, 1926. pages 9

[22] Leonard I. Schiff. *Quantum Mechanics*. International series in pure and applied physics. McGraw-Hill Book Company, New York, 1968. 3rd edition. pages 9

[23] Jeffrey Yepez. A quantum lattice-gas model for computational fluid dynamics. *Physical Review E*, (046702):046702–1 to 046702–18, 2001. APS E-Print: aps1999Oct22_002. pages 11